metals

MDPI

Article

Scandium and Titanium Recovery from Bauxite Residue by Direct Leaching with a Brønsted Acidic Ionic Liquid

Chiara Bonomi [1,*], Alexandra Alexandri [1], Johannes Vind [1,2], Angeliki Panagiotopoulou [3,4], Petros Tsakiridis [1] and Dimitrios Panias [1,*]

1 School of Mining and Metallurgical Engineering, National Technical University of Athens, Iroon Polytechniou 9, Zografou Campus, 15780 Athens, Greece; aalexandri@metal.ntua.gr (A.A.); jvind@metal.ntua.gr (J.V.); ptsakiri@central.ntua.gr (P.T.)
2 Department of Continuous Improvement and System Management, Aluminium of Greece Plant, Metallurgy Business Unit, Mytilineos S.A., Agios Nikolaos, 32003 Viotia, Greece
3 Institute of Biosciences & Applications, National Centre for Scientific Research "Demokritos", Patr. Gregoriou E & 27 Neapoleos Str, Agia Paraskevi, 15310 Athens, Greece; apanagio@bio.demokritos.gr
4 Institute of Biosciences & Applications, National Centre for Scientific Research "Demokritos", Neapoleos 10, Agia Paraskevi, 15310 Athens, Greece
* Correspondence: bonomich@metal.ntua.gr (C.B.); panias@metal.ntua.gr (D.P.); Tel.: +30-210-7724054 (C.B. & D.P.)

Received: 20 September 2018; Accepted: 15 October 2018; Published: 17 October 2018

Abstract: In this study, bauxite residue was directly leached using the Brønsted acidic ionic liquid 1-ethyl-3-methylimidazolium hydrogensulfate. Stirring rate, retention time, temperature, and pulp density have been studied in detail as the parameters that affect the leaching process. Their optimized combination has shown high recovery yields of Sc, nearly 80%, and Ti (90%), almost total dissolution of Fe, while Al and Na were partially extracted in the range of 30–40%. Si and rare earth element (REEs) dissolutions were found to be negligible, whereas Ca was dissolved and reprecipitated as $CaSO_4$. The solid residue after leaching was fully characterized, providing explanations for the destiny of REEs that remain undissolved during the leaching process. The solid residue produced after dissolution can be further treated to extract REEs, while the leachate can be subjected to metal recovery processes (i.e., liquid–liquid extraction) to extract metals and regenerate ionic liquid.

Keywords: bauxite residue; red mud; ionic liquids; scandium recovery; titanium recovery

1. Introduction

Bauxite residue (BR), also known as red mud, is the major byproduct of the Bayer process for alumina production, produced by the alkali leaching of bauxite. On average, for each metric ton of alumina, 1–1.5 metric tons of BR are generated [1,2], which leads to a global production of over 150 million metric tons per year [1,3].

BR composition can differ depending on the type of bauxite ore from which alumina are produced and Bayer processing techniques [4,5]. During the Bayer process, valuable base and trace elements like iron (Fe), some aluminum (Al), titanium (Ti), and rare earth elements (REEs) remain in the bauxite residue. As a consequence, REEs are enriched with a factor of about 2 in BR comparing to the initial ore [6,7]. Particularly interesting is the case of scandium (Sc), as its concentration in BR (in Greek BR accounts to 130 ppm on average) is much higher than in the Earth's crust (22 ppm on average [8]); that means a notable enrichment of Sc in BR. Due to the high market price (Sc_2O_3—4600 US$/kg, 99.99% purity, in 2017) [9], Sc may represent 95% of the economic value of rare earths in BR [10]. It has also

been listed as a critical raw material by the European Commission due to its high economic importance and supply risk [11]. In fact, Sc is mainly produced as a byproduct during the processing of various ores, from titanium and REEs ores (China), uranium ore (Kazakhstan and Ukraine), and apatite ore (Russia). It can also be recovered from previously processed tailings or residues [9,12,13]. For these reasons, BR can be accounted as a secondary raw material source [14], and the recovery of Sc could represent a high economic interest.

BR can also be considered a secondary source for Ti, which is a photocatalyst and it is applied in the white pigment industry [15]. Since the availabilities and qualities of Ti ores are decreasing [16], it is important to find methods for extracting Ti from secondary sources.

Many studies, patents, and pilot scale implementations have been carried out for Sc and Ti recovery from BR, mainly by investigating hydrometallurgical or combined pyro-hydrometallurgical processes [5,12,16–23], but none of them has reached an industrial scale. Nowadays, the impact of the zero-waste valorization policy motivates the research community on finding innovative, greener, and economical viable routes for metal extraction from complex polymetallic matrices, such as the bauxite residue [24].

Ionometallurgical approach can be exploited as an alternative to conventional hydrometallurgical processing. The term ionometallurgy indicates the use of ionic liquids (ILs) as solvents in metals processing. ILs are liquid at room temperature and consist solely of ions; generally an organic cation and inorganic/organic anion. ILs have superior properties against conventional organic solvents, such as nonflammability, a wide electrochemical window, high thermal stability, negligible vapor pressure, and low volatility [25]. For these reasons and thanks to the vast number of combinations of the cation and the anion during synthesis, ILs have potential for many applications, such as solvent extraction [26,27], catalytic reactions [28,29], and electrodeposition of metals [30,31]. In the past few decades, ILs have been used also as lixiviants for metals dissolution [25,32–35]. Applying ionic liquid leaching on secondary raw material resources eventually improves efficiency yields, reduce waste effluent, and increases selectivity.

The aim of this work is to investigate the direct leaching of bauxite residue by using a Brønsted acidic ionic liquid, achieving high Ti and Sc recovery yields. To optimize the process, several parameters were studied. Moreover, solid residue after leaching was fully characterized and explanations of the destiny of REEs were given.

2. Materials and Methods

Bauxite residue was provided by Aluminium of Greece (Mytilineos S.A.), dried at 100 °C overnight, homogenized, and split in order to take a representative sample that was next crushed and ground. The sample was then subjected to chemical, mineralogical and physical characterization. Chemical composition was analyzed after complete dissolution of the sample via fusion method: 0.1 g of BR was mixed with 1.5 g of $Li_2B_4O_7$ and 0.1 g of KNO_3 and then fused at 1000 °C for 1 h, followed by dissolution in HNO_3 10% v/v. The main elements were identified by a Perkin Elmer 2100 Atomic Absorption Spectrometer (AAS) (Waltham, MA, USA), while minor elements were analyzed by a Thermo Fisher Scientific™ X-series 2 Inductively Coupled Plasma Mass Spectrometer (ICP-MS) (Waltham, MA, USA) and a Perkin Elmer Optima 8000 Inductively Coupled Plasma Atomic Emission Spectrometer (ICP-OES) (Waltham, MA, USA). The calcium oxide content was measured in the solid sample with a Spectro Xepos Energy Dispersive X-ray fluorescence spectroscopy (SPECTRO, Kleve, Germany) (ED-XRF). Mineralogical characterization was performed with a Bruker D8 focus X-ray powder diffractometer (XRD) (Bruker, Billerica, MA, USA) with nickel-filtered CuKa radiation, and quantitative evaluation was done via profile fitting by using XDB Powder Diffraction Phase Analytical System version 3.107 that targets specifically bauxite and bauxite residue [36,37]. Particle size analysis was carried out by a Malvern Mastersizer TM Laser particle size analyzer (Malvern Instruments, Malvern, UK).

The ionic liquid 1-ethyl-3-methylimidazolium hydrogensulfate ([Emim][HSO_4]) was supplied by Iolitec (Iolitec Ionic Liquids Technologies, Heilbronn, Germany) with >98% purity and characterized. Infrared measurements were conducted with a Perkin Elmer FTIR spectrum 100 (Waltham, MA, USA). Viscosity analysis was performed with a Brookfield viscometer DV-I + LV supported by a Brookfield Thermosel accessory (Brookfield Ametek, Harlow, UK). Nuclear Magnetic Resonance (NMR) spectra were obtained in DMSO-d_6 at 25 °C on a Bruker Avance DRX 500 MHz (Bruker Biospin, Germany) (^{1}H at 500.13 MHz and ^{13}C at 125.77 MHz) equipped with a 5 mm multi nuclear broad band inverse detection probe.

Batch leaching experiments were performed in a 50 mL Trallero and Schlee mini reactor (Trallero and Schlee, Barcelona, Spain) combined with a mechanical stirrer, a vapor condenser, and a temperature controller, by adding BR to the IL when the set temperature was reached. Vacuum filtration was executed by cooling the system at 120 °C and adding a nonviscous/volatile solvent (dimethyl sulfoxide, further denoted as DMSO) to the leachates, to decrease viscosity and ease the process. After filtration, pregnant leaching solutions (PLS) were digested through acidic treatment (HNO_3 65% v/v and aqua regia) to oxidize and destroy the organics and then analyze with AAS, ICP-OES and ICP-MS. Solid residues were characterized via fusion method (already described above) and XRD. Microstructural characterization was carried out by a JEOL 6380 LV Scanning Electron Microscope (JEOL, Tokyo, Japan) coupled with Energy Dispersive System (SEM-EDS) and a JEOL 2100 HR (JEOL, Tokyo, Japan) 200 kV Transmission Electron Microscope (TEM) in order to detect and locate REEs.

3. Results and Discussion

3.1. Bauxite Residue Characterization

The main component of BR was found to be Fe_2O_3, accounting for 42.34 wt.%, followed by Al_2O_3 with 16.25 wt.%, while TiO_2 was 4.27 wt.%, and total rare earth oxides (REO) assessed to 0.19 wt.%, as it is shown in Table 1.

Table 1. Bauxite residue chemical analysis. Note: REO, rare earth oxides; LOI, loss of ignition.

Unit	Fe_2O_3	Al_2O_3	SiO_2	TiO_2	CaO	Na_2O	REO	LOI	Others	Sum
wt.%	42.34	16.25	6.97	4.27	11.64	3.83	0.19	12.66	1.85	100.00

In particular, cerium (Ce) was found to be the main rare earth element in concentration (402.2 mg/kg), followed by lanthanum (La) (145 mg/kg), scandium (Sc) (134 mg/kg), neodymium (Nd) (127.1 mg/kg), and yttrium (Y) (112 mg/kg).

Identification and quantification of mineralogical phases (Table 2) denoted hematite as the main mineral in BR with 30 wt.%, while Ti-containing phases were perovskite, anatase and rutile with 4.5, 0.5 and 0.5 wt.% respectively.

Table 2. Bauxite residue mineralogical phases and quantification.

Mineralogical Phase	Formula	wt.%
Hematite	Fe_2O_3	30
Calcium aluminum iron silicate hydroxide	$Ca_3AlFe(SiO_4)(OH)_8$	17
Cancrinite	$Na_6Ca_2(AlSiO_4)_6(CO_3)_2$	15
Diaspore	α-AlOOH	9
Goethite	$Fe_2O_3{\cdot}H_2O$	9
Perovskite	$CaTiO_3$	4.5
Chamosite	$(Fe^{2+},Mg)_5Al(AlSi_3O_{10})(OH)_8$	4
Calcite	$CaCO_3$	4
Boehmite	γ-AlOOH	3
Gibbsite	$Al(OH)_3$	2
Rutile	TiO_2	0.5
Anatase	TiO_2	0.5
Sum		98.5

From particle size distribution analysis, it was found that 50% of the particles were below 1.87 μm, while 90% were smaller than 42.87 μm.

3.2. Ionic Liquid Characterization

1-ethyl-3-methylimidazolium hydrogensulfate ([Emim][HSO_4]) is a Brønsted acidic ionic liquid whose molecular weight is 208.24 g/mol and density (ρ) at room temperature is 1367.9 kg/m^3. The molecular structure of the IL is shown in Figure 1.

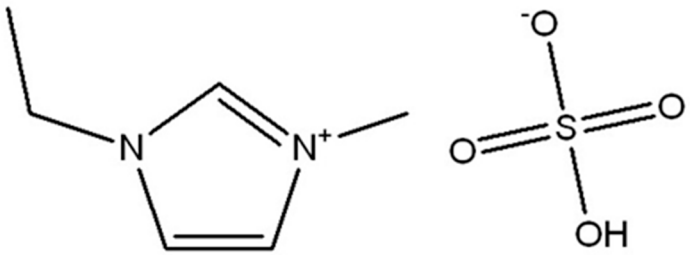

Figure 1. [Emim][HSO_4] molecular structure.

Viscosity measurements (Figure 2) have revealed that even though [Emim][HSO_4] is very viscous at room temperature (1642 mPa·s), by increasing temperature its viscosity dramatically decreases, reaching 221 mPa·s at 60 °C and 33 mPa·s at 120 °C.

Midinfrared spectrum have shown bands (cm^{-1}) at 3452 (OH), 3151 (aromatic/imidazole CH), 3106 (imidazole ring), 2985 (CH), 2944 (CH), 2881 ((CH_2)$_n$–CH_3), 2583–2497 (HOSO●●●HOSO), 1636 (OH), 1572 (C=C, C=N, C–N), 1454 (CH_3), 1431 (S=O_2), 1389 (CH_3), 1211 (S=O_2), 1160 (S–O attached to C_2H_5), 1089 (HSO_4^-), 1023 (C–N–C), 960 (O–S–O), 832 (imidazole ring), 757 (CH of imidazole ring) and 701 (C–H–C). ^{1}H NMR (500 MHz, DMSO) δ (ppm): 1.36 (t, 3H, CH_3), 3.85 (s, 3H, CH_3), 4.19 (q, 2H, CH_2), 7.71 (s, 1H, CH=CH), 7.78 (s, 1H, CH=CH), 9.19 (s, 1H, N–CH–N).

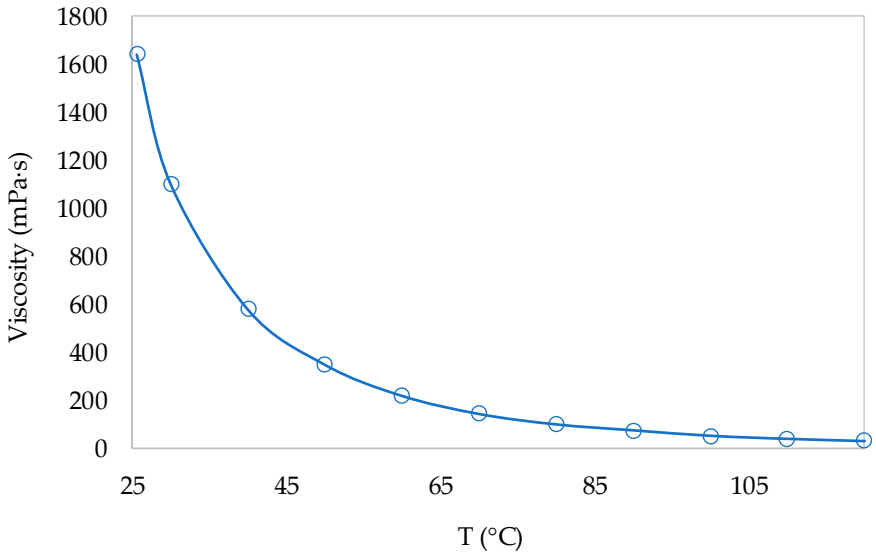

Figure 2. Viscosity measurements of [Emim][HSO_4] versus temperature.

Reaction Mechanism

To investigate the mechanism of the reaction that takes place, two monometallic solutions of 11 g/L of Sc and 11 g/L of Al were prepared, by dissolving Sc_2O_3 and Al_2O_3 in [Emim][HSO_4].

The two monometallic solutions were then analyzed with ^{1}H and ^{13}C NMR. Assignment of ^{1}H and ^{13}C chemical shifts was based on the combined analyses of a series of ^{1}H–^{1}H and ^{1}H–^{13}C correlation experiments recorded using standard pulse sequences from the Bruker library.

From the results (Appendix A, Figures A1 and A2), it could be concluded that there is no significant rearrangement in the carbon chain after the dissolution procedure in all three metal cases.

^{1}H and ^{13}C NMR spectra did not indicate any notable differences in the chemical shifts depending on the leached metal. The similar chemical shifts for the protons and the carbons localized in between the two nitrogen atoms indicate metal interaction through the anion of the IL.

There is not any steric effect of electron clouds changing of electrostatic interactions between ionic charges.

The results obtained from NMR analysis of two monometallic leachates have led to the following proposed reaction:

$$Me_2O_n + n[Emim][HSO_4] = Me_2(SO_4)_n + nOH^- + n[Emim]^+ \quad (1)$$

where Me is the metal and n is the oxidation state of the metal.

3.3. Leaching Process Optimization: Parameters Affecting the System

In order to optimize the process, stirring rate, retention time, temperature, and pulp density were investigated. Each parameter was studied separately, keeping the others constant, and choosing the combination that gave the best results. In each case, Ca and Si in leachates were below the detection limit and Ce, Nd, Y and La recovery was lower than 1%.

3.3.1. Stirring Rate

Initially, experiments were carried out by examining four different stirring rates, 100, 200, 400 and 600 revolutions per minute (rpm), while keeping constant all the other parameters at 150 °C, 5% *w*/*v* pulp density and 24 h. Results are given in Figure 3.

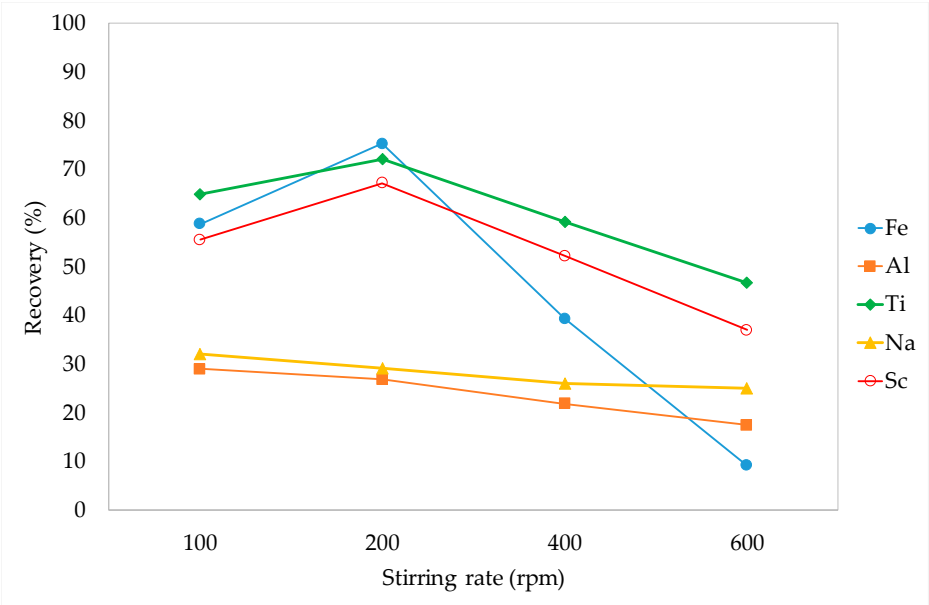

Figure 3. Investigation of the stirring rate effect on metals dissolution by leaching BR with [Emim][HSO_4] at 150 °C, 5% *w*/*v* pulp density for 24 h.

At these conditions, it is possible to observe an increase of Fe, Ti, and Sc extraction when the stirring rate increases from 100 to 200 rpm (from 55% of Sc, 57% of Fe, and 65% of Ti at 100 rpm to 67% of Sc, 75% of Fe and 72% of Ti at 200 rpm). On the other hand, as the stirring rate increases from 200 to 600 rpm, Fe, Ti, and Sc extraction is observed to linearly decrease (from 67% of Sc, 75% of Fe, and 72% of Ti at 200 rpm to 37% of Sc, 46% of Ti, and only 9% for Fe at 600 rpm). Na and Al recovery were

slightly affected by the stirring rate as they remained almost stable in a range of 17–32% of recovery. This effect of stirring rate on metal recovery is typical in hydrometallurgy. Under low stirring rates, a thick boundary layer was developed on the surface of the solid particles, making the diffusion of chemical species from and to the solid particles surface inefficient. Therefore, at stirring rates lower than 200 rpm, the leaching process is slowed down and metal recovery decreases, as it is seen in Figure 3. At stirring rates higher than 200 rpm, the thickness of the boundary layer is substantially decreased, but the high convective mass transfer of reactants from the surface of the particles, makes the surface reactions again inefficient and thus the recovery yields are diminishing, as it is seen in Figure 3. Therefore, a compromise is always found under intermediate stirring rates which, for this system, is around 200 rpm. At this stirring rate, Fe, Ti, and Sc have the highest recovery yields (75%, 72% and 67% respectively).

3.3.2. Kinetic Studies

Several sets of kinetic have been performed at 200 rpm stirring rate, 5% w/v pulp density, analyzing the behavior of the system at three different temperatures: 150, 175, and 200 °C.

In Figure 4 it is observed that at low temperature (150 °C), all metals show the same trend in the first twelve hours; an initial metal dissolution occurred in the first six hours, whilst in the following six hours, metals dissolution is decreased, reaching their lowest concentration at 12 h retention time. This unusual behavior can be attributed to the precipitation of Ca as $CaSO_4$ that massively occurs within the first 6 h (Appendix A, Figure A3), while Fe dissolution is low. In the latter 6 h, adsorption phenomena were more important and faster than dissolution and, being in contact with anhydrite, metals are removed from the leachates, attaining the minimum at 12 h. Then, metals continue their dissolution and as the anhydrite precipitation has been completed they are gradually desorbed, increasing their concentration in solution and reaching the equilibrium at 24 h retention time, with the exception of iron that continues to be dissolved but at a substantially lower rate.

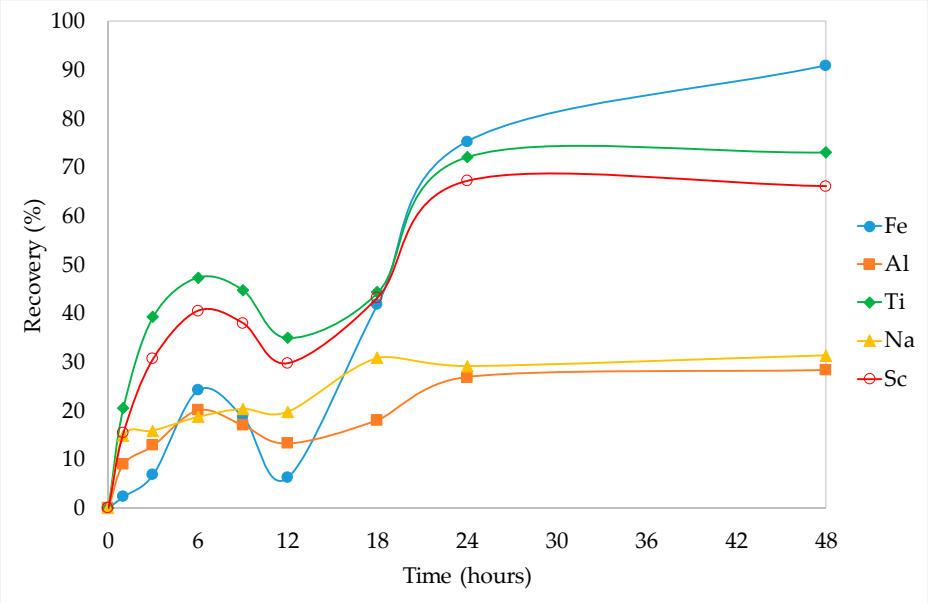

Figure 4. Kinetic curves for metals dissolution by leaching BR with [Emim][HSO_4] at 1, 3, 6, 12, 18, 24 and 48 h, 200 rpm, 150 °C and 5% w/v pulp density.

Kinetic studies have been carried out at 175 °C (Figure 5), in this case the unusual dissolution phenomenon observed at 150 °C was not seen and the plateau has been reached faster, after 12 h, achieving 90% of Fe, 70% of Ti and Sc dissolution and again moderate Al and Na recovery (30%). After 1 h, more than 35% of Sc has been dissolved, this, as mentioned, is due to the fact that goethite

is totally dissolved and hematite starts to be leached as well. The equilibrium has been reached at 70% of Sc and 90% of Fe recovery, which is in agreement with Vind et al. studies, as the main mineralogical Sc containing phases in bauxite residue are hematite and goethite (55% and 25% on average, respectively) [38].

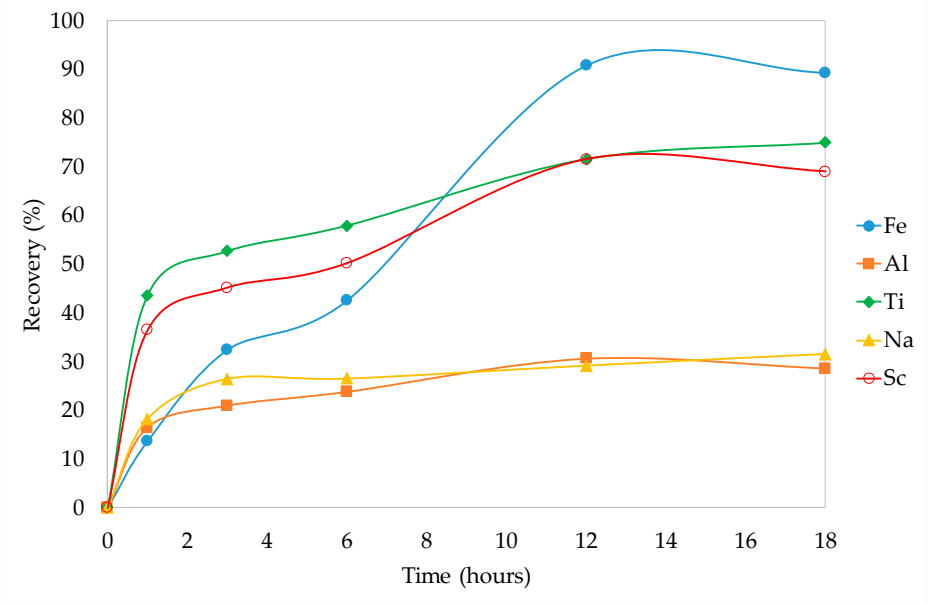

Figure 5. Kinetic curves for metals dissolution by leaching BR with [Emim][HSO_4] at 1, 3, 6, 12, and 18 h, 200 rpm, 175 °C and 5% *w*/*v* pulp density.

At 200 °C (Figure 6), Fe, Ti and Sc are considerably leached even after 1 h (60–74%). The maximum extraction of these metals has been reached after 12 h, where Fe was almost totally dissolved, Ti recovery was over 90% and Sc reached nearly 80%. Al and Na dissolution remained stable along the kinetic curve in a range of 30–40%.

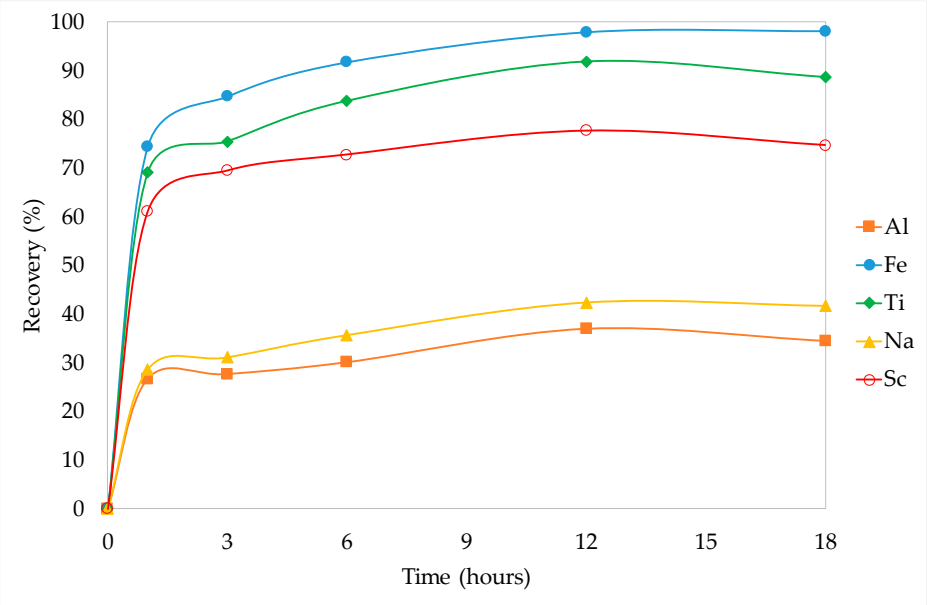

Figure 6. Kinetic curves for metals dissolution by leaching BR with [Emim][HSO_4] at 1, 3, 6, 12, and 18 h, 200 rpm, 200 °C, and 5% *w*/*v* pulp density.

Extraction of Sc at these high recovery yields (nearly 80%), when Fe was also almost totally dissolved, again confirms that Sc was found to be hosted mainly in hematite and goethite mineralogical phases in bauxite residue [38], as already mentioned. It was hypothesized before that in the same experimental setup as given here, the unrecovered proportion of Sc (about 20%) may be associated mainly with the chemically durable zirconium orthosilicate ($ZrSiO_4$), that contains around 10% of the total Sc in bauxite residue, but also with other undissolved (or partially dissolved) phases as boehmite, diaspore, and titanium-containing phases, which have been determined to be carriers of Sc in Greek BR [38].

3.3.3. Pulp Density

Four experiments have been conducted to investigate the effect of pulp density on the system, at 2.5%, 5%, 10%, and 14.3% w/v pulp density, under constant temperature, time and stirring rate (200 °C, 12 h, and 200 rpm). Results are shown in Figure 7.

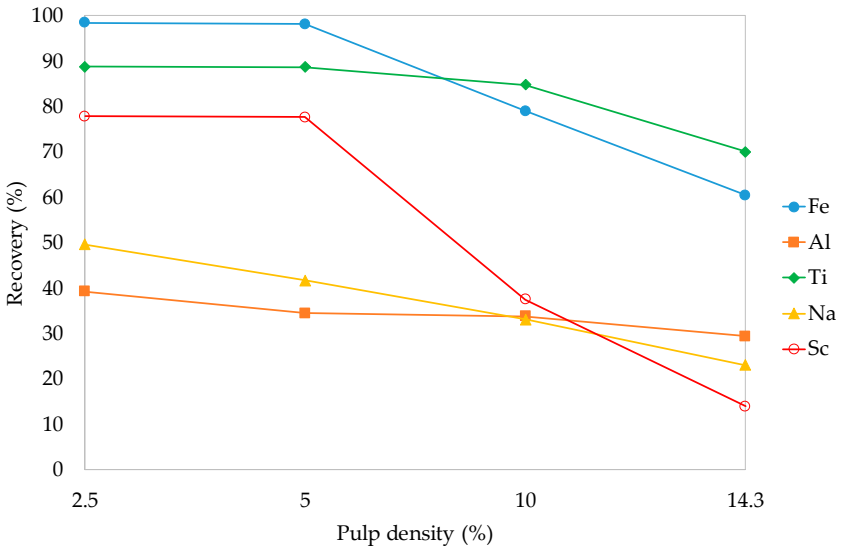

Figure 7. Study on the system behavior for metals dissolution by changing pulp density when leaching BR with [Emim][HSO_4] at 12 h, 200 rpm, 200 °C.

Fe, Ti, and Sc present constant recovery in the area of 2.5–5% w/v pulp density (almost total dissolution for Fe, 88% for Ti, and 78% for Sc). This behavior can be explained by the extremely high ionic liquid excess and the relatively low viscosity of the system due to the low concentration of dissolved metals. By increasing pulp density, the ionic liquid excess decreases and viscosity substantially rises, due to the increase of the number of suspended BR particles as well as the dissolved metal concentrations affecting the ions mobility phenomena and the thickness of the boundary layer. This results in a sharp and linear decreasing recovery, reaching the minimum at 14.3% w/v (60% of Fe, 70% Ti, and 14% of Sc). Experiments at pulp density higher than 14.3% w/v were not carried out due to the high viscosity, which prevented filtration and caused serious problems during the leaching process.

3.4. Characterization of the Solid Residue after Leaching

The solid residue collected after leaching bauxite residue at optimum conditions (200 rpm, 200 °C, 12 h and 5% w/v pulp density) was characterized via fusion method, XRD, SEM, and TEM analyses. The resulting residue was found to be 48% of the weight of the initial BR mass.

As it can be seen from chemical analysis shown in Table 3, solid residue after leaching is high in aluminum, calcium, and silicon, while it is depleted in iron and titanium. REEs remain in the solid residue (with the exception of scandium) and can be leached afterwards.

Table 3. Chemical analysis of the residue after leaching BR at optimum conditions.

Metal Oxide	Fe_2O_3	Al_2O_3	SiO_2	TiO_2	CaO	Na_2O	REO	SO_3	LOI	Others
wt.%	3.71	27.44	14.51	1.46	24.73	2.75	0.19	18.69	6.00	0.52

From the comparison of the XRD spectra of bauxite residue and residue generated after leaching (Appendix A, Figure A4), it is possible to observe that peaks attributed to hematite, goethite, calcium aluminum iron silicate hydroxide, gibbsite, and perovskite, which are present in bauxite residue, disappear after leaching. Aluminum phases like diaspore and boehmite remain relatively intact after leaching, as well as cancrinite, chamosite, and calcite. On the other hand, a new mineralogical phase calcium sulfate anhydrite (causing the consumption of about 2 wt.% of the IL), which was formed due to the interaction between calcium and the anion of the ionic liquid, is created during leaching. The above observations explain well the behavior of Al and Na during leaching as their main minerals in BR such as diaspore, boehmite and cancrinite remain insoluble, leading to low to moderate recoveries. On the other hand, Fe and Ti bearing minerals were depleted in leaching residue thus confirming their observed high recoveries. Regarding Ca leaching, phases like calcium aluminum iron silicate hydroxide are substantially soluble, while phases such as cancrinite and chamosite resist dissolution. Calcite is partially dissolved in IL solution and in the presence of HSO_4^- anions, undertakes a transition to anhydrite, which is a secondary precipitated phase during the leaching process.

SEM-EDS analysis of the solid residue after leaching confirmed the findings of chemical and XRD analyses (Figure 8). The matrix, which is mainly composed of Al, Ca, and Na silicates, surrounds phases transitioning from $CaCO_3$ to $CaSO_4$.

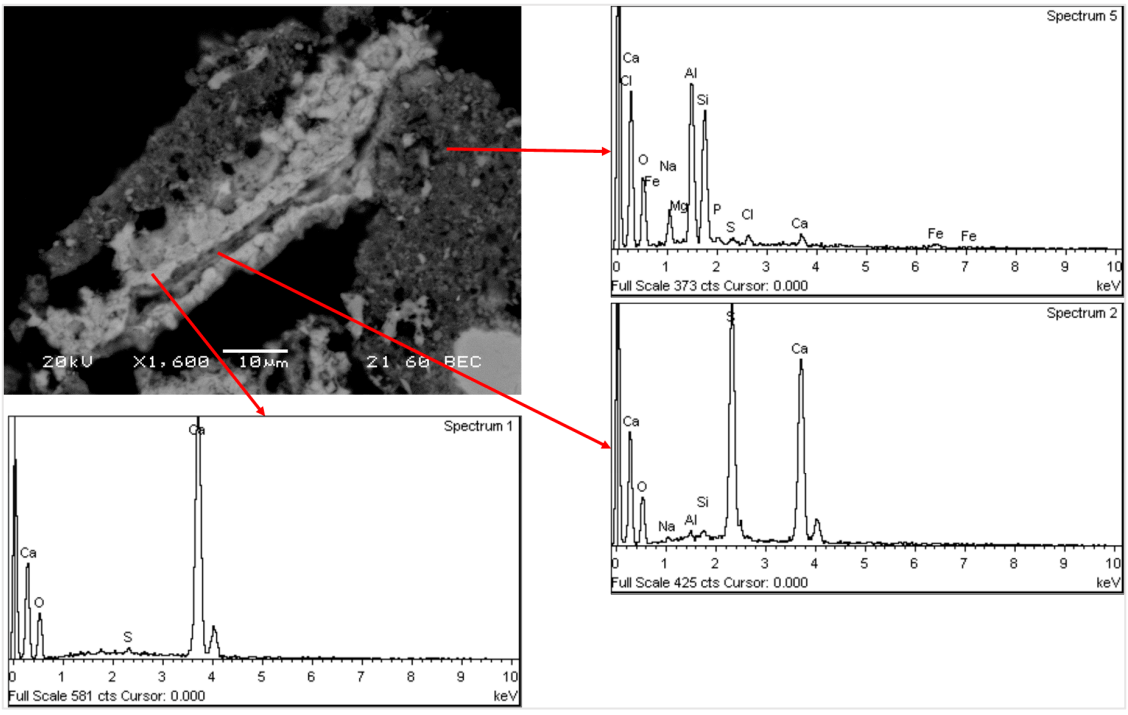

Figure 8. Scanning electron microscope (SEM image of the matrix of the residue after leaching).

3.5. REEs in the Solid Residue

Small REEs-containing particles (about 10 µm) were detected in SEM-EDS, in particular YPO_4 particles including heavy rare earths like gadolinium and dysprosium (Figure 9 left). This is consistent with Vind et al. studies of raw bauxite residue [39] where the presence of heavy rare earth phosphates with the major constituent being yttrium and containing other heavy REEs like

gadolinium, dysprosium, and erbium is reported. This is an indication that these grains endure the [Emim][HSO_4] leaching process without being subjected to any dissolution and thus explaining negligible heavy REEs recoveries.

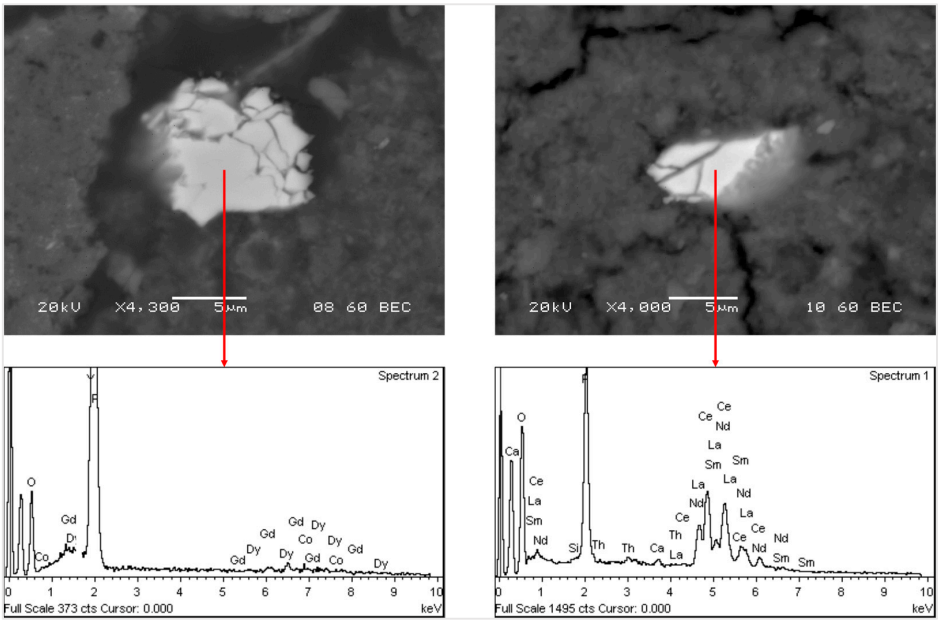

Figure 9. SEM image of a YPO_4 particle (**left**) and a $CePO_4$ particle (**right**).

Small mixed calcium–cerium phosphate particles were also identified; in this case, grains included light rare earths like neodymium, lanthanum, and samarium (Figure 9 right). Vind et al. reported the presence of light rare earths as calcium-containing phosphate phases in bauxite residue [39]. In the case of the solid residue after leaching, grains containing light REEs (LREEs) phosphates are also present. This may indicate a partial dissolution of calcium from the mixed Ca-LREEs phases, leaving behind smaller phosphate particles which are beneficiated in LREEs. This was also implied by TEM analysis, detecting very fine (<500 nm) particles of Al-containing $CePO_4$ (Figure 10).

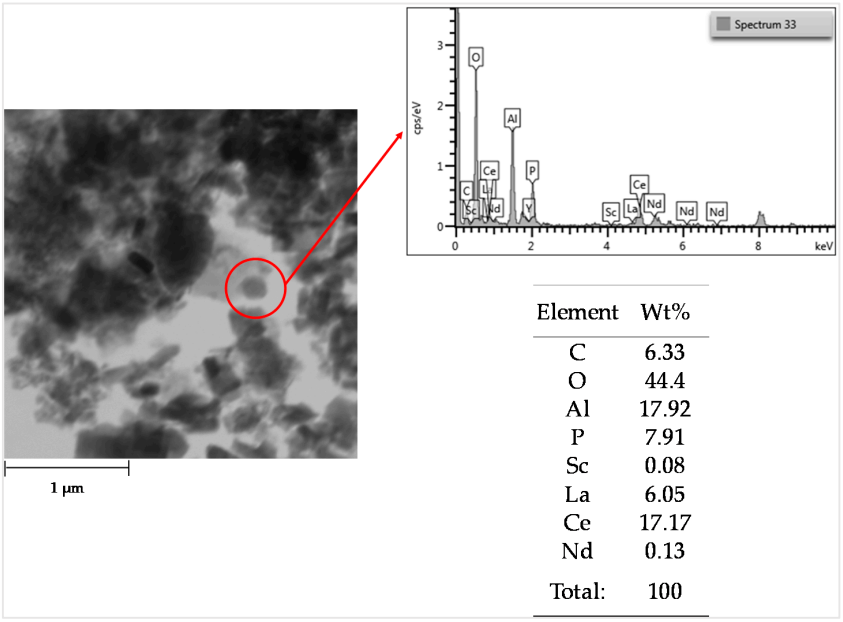

Element	Wt%
C	6.33
O	44.4
Al	17.92
P	7.91
Sc	0.08
La	6.05
Ce	17.17
Nd	0.13
Total:	100

Figure 10. TEM image of a $CePO_4$, Al containing, particle.

4. Conclusions

In this study, Brønsted acidic ionic liquid 1-ethyl-3-methylimidazolium hydrogensulfate was used to directly leach bauxite residue. Experiments were carried out in a closed mini reactor, equipped with a condenser and a temperature controller. Stirring rate, time, temperature and pulp density were thoroughly examined to find the optimum conditions for Sc (nearly 80%) and Fe (almost totally dissolved) high recovery yields. This outcome confirms that Sc is mainly hosted in hematite and goethite mineralogical phases (55% and 25%, respectively) in bauxite residue, in accordance to the work of Vind et al. [38]. The undissolved Sc content might be attributed to $ZrSiO_4$, containing around 10% of the total Sc in bauxite residue, but also to other phases, such as boehmite, diaspore, and titanium-containing phases that host Sc in Greek bauxite residue [38].

At the optimum conditions, 90% of Ti was dissolved, while Al and Na were partially extracted (in a range of 30–40%). Si and REEs dissolutions were found to be negligible, whereas Ca was partially dissolved and precipitated as $CaSO_4$ consuming about 2 wt.% of the ionic liquid.

Solid residue after leaching was fully characterized and found to be rich in Al, Ca, and Si, with the main minerals present being anhydrite, diaspore, and cancrinite; it could be further treated to extract REEs. SEM and TEM analyses of the solid residues provided explanations for the destiny of REEs, which remain undissolved enduring the leaching process.

It can be concluded that [Emim][HSO_4] ionic liquid is a good leaching agent for dissolving metals from bauxite residue and, since it is not selective against iron, high recovery yields of Sc can be achieved, reaching up to 80% of extraction.

Author Contributions: C.B. and D.P. conceived and designed the experiments; C.B. performed the experiments; A.P. performed NMR analysis and analyzed the spectra; A.A. performed chemical analyses; J.V. and C.B. performed the SEM-EDS analysis and analyzed the data; P.T. performed TEM analysis; C.B. analyzed the data and wrote the paper; D.P. contributed to the analysis of the data and the writing of the paper.

Acknowledgments: The research leading to these results has received funding from the European Community's Horizon 2020 Program (H2020/2014—2019) under Grant Agreement no. 636876 (MSCA–ETN REDMUD).

Conflicts of Interest: The authors declare no conflict of interest. The funding sponsors had no role in the design of the study; in the collection, analyses, or interpretation of data; in the writing of the manuscript, and in the decision to publish the results.

Appendix A

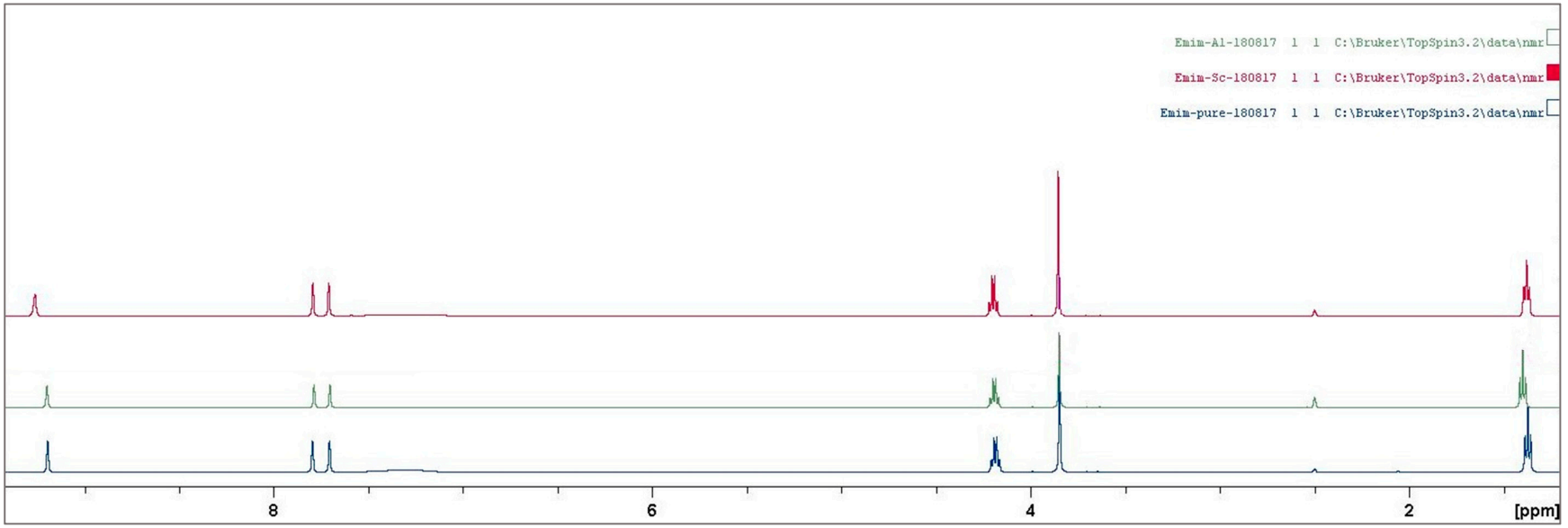

Figure A1. ^{1}H Nuclear Magnetic Resonance (NMR) comparison between [Emim][HSO_4] (blue), [Emim][HSO_4] after leaching Al_2O_3 (green), [Emim][HSO_4] after leaching Sc_2O_3 (red).

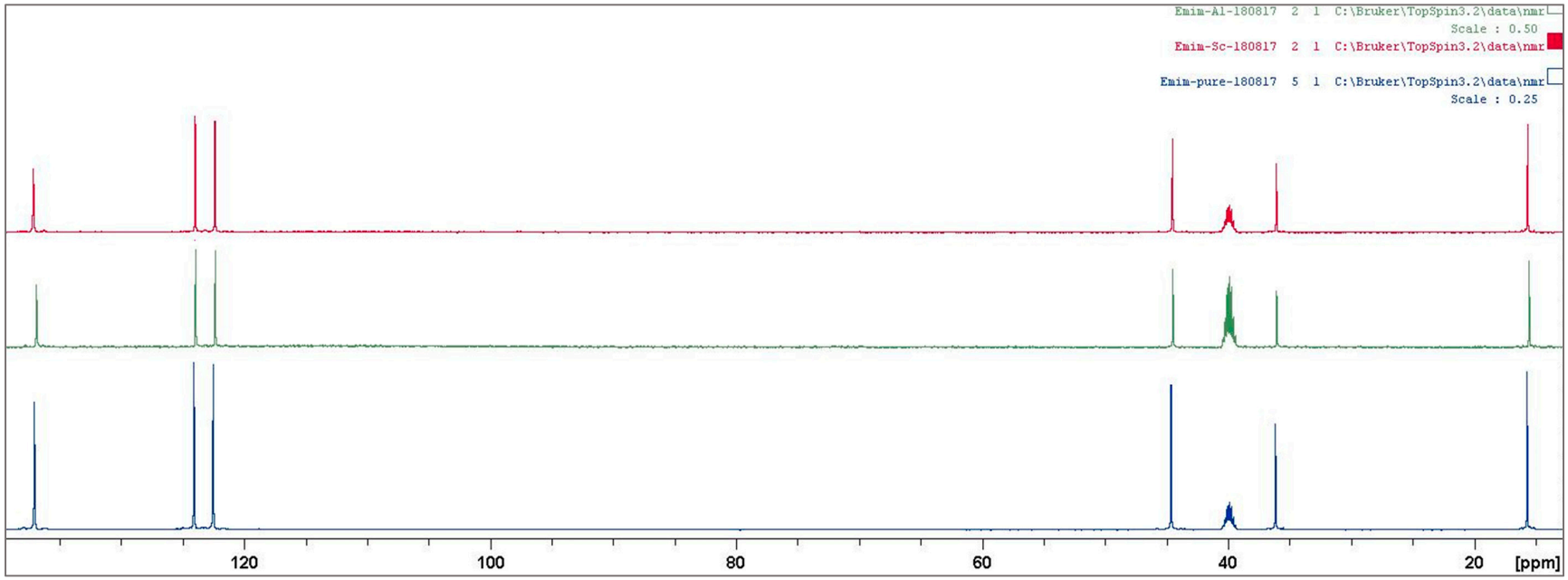

Figure A2. ^{13}C NMR comparison between [Emim][HSO_4] (blue), [Emim][HSO_4] after leaching Al_2O_3 (green), [Emim][HSO_4] after leaching Sc_2O_3 (red).

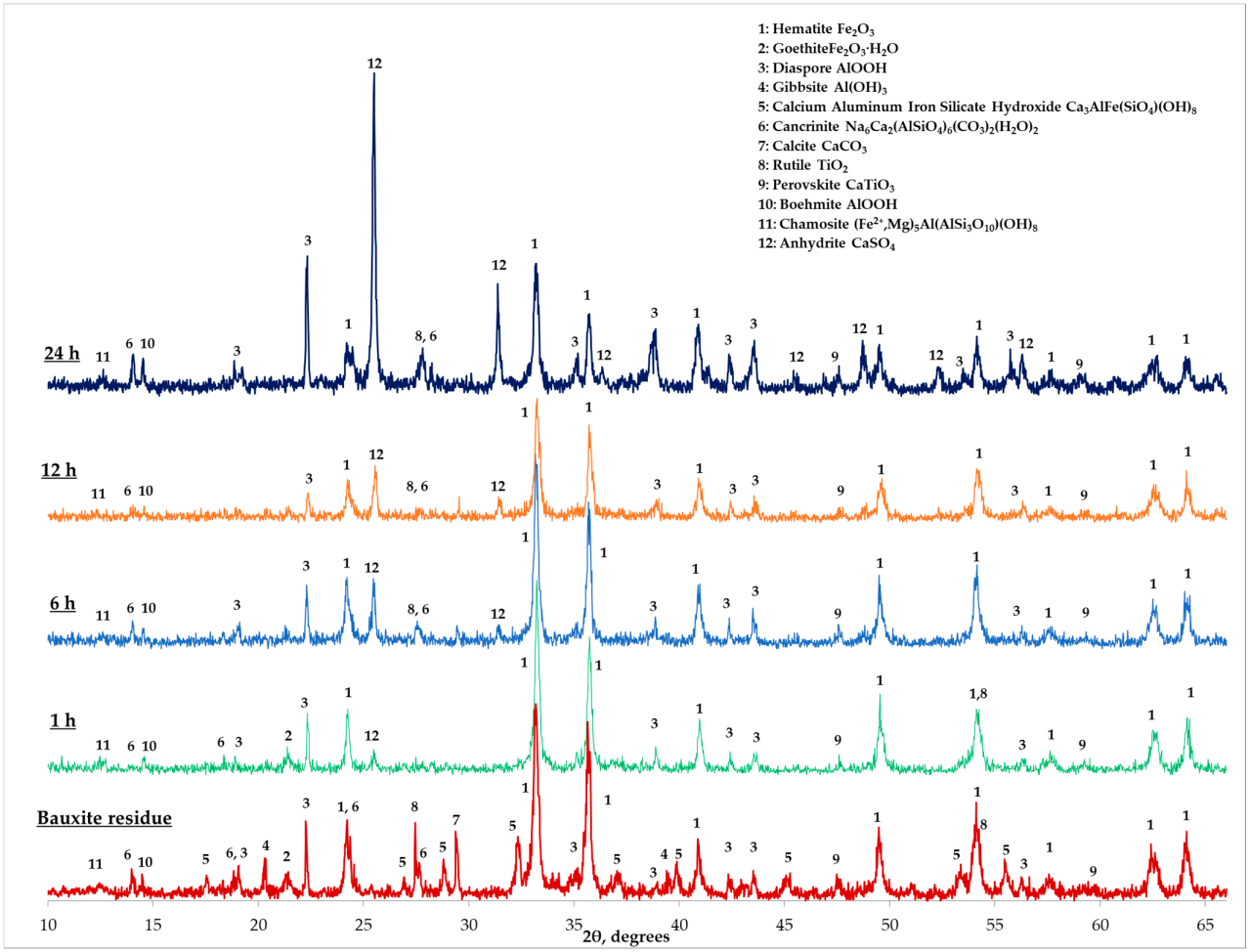

Figure A3. Comparison between X-ray powder diffractometer (XRD) of bauxite residue and solid residue after leaching bauxite residue at 150 °C, 200 rpm, 5% *w*/*v* pulp density for 1, 6, 12, and 24 h.

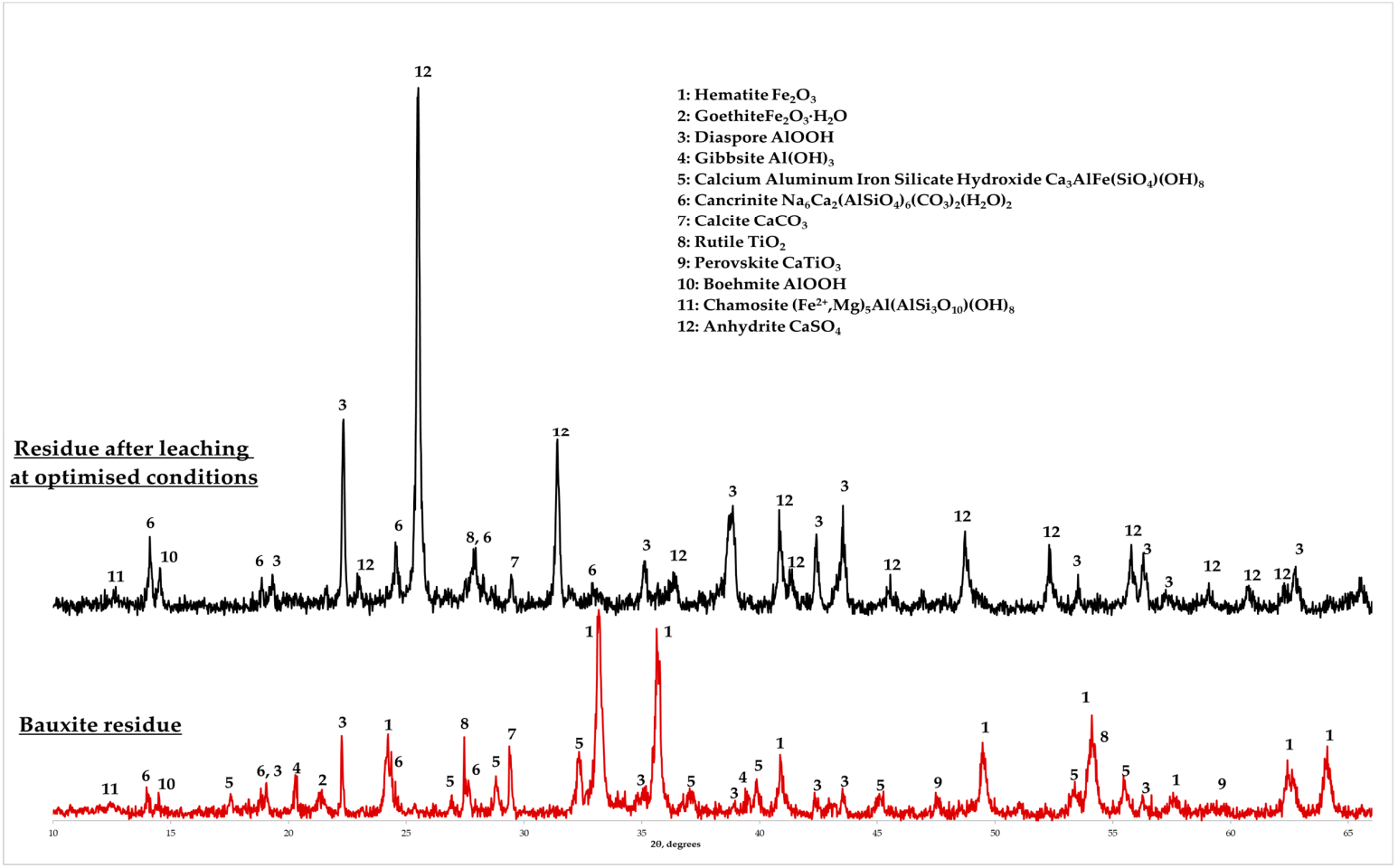

Figure A4. Comparison of the XRD spectra of bauxite residue and solid residue after leaching at optimum conditions.

References

1. Evans, K. The History, Challenges, and New Developments in the Management and Use of Bauxite Residue. *J. Sustain. Metall.* **2016**, *2*, 316–331. [CrossRef]
2. Zhang, R.; Zheng, S.; Ma, S.; Zhang, Y. Recovery of Alumina and Alkali in Bayer Red Mud by the Formation of Andradite-Grossular Hydrogarnet in Hydrothermal Process. *J. Hazard. Mater.* **2011**, *189*, 827–835. [CrossRef] [PubMed]
3. Klauber, C.; Gräfe, M.; Power, G. Bauxite Residue Issues: II. Options for Residue Utilization. *Hydrometallurgy* **2011**, *108*, 11–32. [CrossRef]
4. Gräfe, M.; Power, G.; Klauber, C. Bauxite Residue Issues: III. Alkalinity and Associated Chemistry. *Hydrometallurgy* **2011**, *108*, 60–79. [CrossRef]
5. Liu, Y.; Naidu, R. Hidden Values in Bauxite Residue (Red Mud): Recovery of Metals. *Waste Manag.* **2014**, *34*, 2662–2673. [CrossRef] [PubMed]
6. Ochsenkühn-Petropulu, M.; Lyberopulu, T.; Parissakis, G. Direct Determination of Landthanides, Yttrium and Scandium in Bauxites and Red Mud from Alumina Production. *Anal. Chim. Acta* **1994**, *296*, 305–313. [CrossRef]
7. Vind, J.; Alexandri, A.; Vassiliadou, V.; Panias, D. Distribution of Selected Trace Elements in the Bayer Process. *Metals (Basel)* **2018**, *8*, 327. [CrossRef]
8. Rudnick, R.L.; Gao, S. Composition of the Continental Crust. In *Treatise on Geochemistry*; Elsevier: Amsterdam, The Netherlands, 2003; pp. 1–64.
9. Gambogi, J. *Mineral Commodity Summaries, Scandium*; U.S. Geological Survey: Reston, VA, USA, 2017; pp. 146–147.
10. Balomenos, E.; Davris, P.; Pontikes, Y.; Panias, D. Mud2Metal: Lessons Learned on the Path for Complete Utilization of Bauxite Residue Through Industrial Symbiosis. *J. Sustain. Metall.* **2017**, *3*, 551–560. [CrossRef]
11. Deloitte Sustainability; British Geological Survey; Bureau de Recherches Géologiques et Minières; TNO. *Study on the Review of the List of Critical Raw Materials*; EU Law and Publications: Luxembourg, 2017; ISBN 978-92-79-47937-3.
12. Borra, C.R.; Blanpain, B.; Pontikes, Y.; Binnemans, K.; Van Gerven, T. Recovery of Rare Earths and Other Valuable Metals From Bauxite Residue (Red Mud): A Review. *J. Sustain. Metall.* **2016**, *2*, 365–386. [CrossRef]
13. Ochsenkühn-Petropulu, M.; Lyberopulu, T.; Parissakis, G. Selective Separation and Determination of Scandium from Yttrium and Lanthanides in Red Mud by a Combined Ion Exchange/Solvent Extraction Method. *Anal. Chim. Acta* **1995**, *315*, 231–237. [CrossRef]
14. Binnemans, K.; Jones, P.T.; Blanpain, B.; Van Gerven, T.; Pontikes, Y. Towards Zero-Waste Valorisation of Rare-Earth-Containing Industrial Process Residues: A Critical Review. *J. Clean. Prod.* **2015**, *99*, 17–38. [CrossRef]
15. Bonomi, C.; Cardenia, C.; Yin, P.T.W.; Panias, D. Review of Technologies in the Recovery of Iron, Aluminium, Titanium and Rare Earth Elements from Bauxite Residue (Red Mud). In Proceedings of the International Symposium on Enhanced Landfill Mining, Lisboa, Portugal, 8–10 February 2016; pp. 259–276.
16. Alkan, G.; Schier, C.; Gronen, L.; Stopic, S.; Friedrich, B. A Mineralogical Assessment on Residues after Acidic Leaching of Bauxite Residue (Red Mud) for Titanium Recovery. *Metals* **2017**, *7*, 458. [CrossRef]
17. Agatzini-Leonardou, S.; Oustadakis, P.; Tsakiridis, P.E.; Markopoulos, C. Titanium Leaching from Red Mud by Diluted Sulfuric Acid at Atmospheric Pressure. *J. Hazard. Mater.* **2008**, *157*, 579–586. [CrossRef] [PubMed]
18. Alkan, G.; Yagmurlu, B.; Cakmakoglu, S.; Hertel, T.; Kaya, Ş.; Gronen, L.; Stopic, S.; Friedrich, B. Novel Approach for Enhanced Scandium and Titanium Leaching Efficiency from Bauxite Residue with Suppressed Silica Gel Formation. *Sci. Rep.* **2018**, *8*, 5676. [CrossRef] [PubMed]
19. Liu, Z.; Li, H. Metallurgical Process for Valuable Elements Recovery from Red Mud—A Review. *Hydrometallurgy* **2015**, *155*, 29–43. [CrossRef]
20. Ochsenkühn-Petropoulou, M.T.; Hatzilyberis, K.S.; Mendrinos, L.N.; Salmas, C.E. Pilot-Plant Investigation of the Leaching Process for the Recovery of Scandium from Red Mud. *Ind. Eng. Chem. Res.* **2002**, *41*, 5794–5801. [CrossRef]
21. Ochsenkühn-Petropulu, M.; Lyberopulu, T.; Ochsenkühn, K.M.; Parissakis, G. Recovery of Lanthanides and Yttrium from Red Mud by Selective Leaching. *Anal. Chim. Acta* **1996**, *319*, 249–254. [CrossRef]

22. Borra, C.R.; Blanpain, B.; Pontikes, Y.; Binnemans, K.; Van Gerven, T. Smelting of Bauxite Residue (Red Mud) in View of Iron and Selective Rare Earths Recovery. *J. Sustain. Metall.* **2016**, *2*, 28–37. [CrossRef]
23. Borra, C.R.; Pontikes, Y.; Binnemans, K.; Van Gerven, T. Leaching of Rare Earths from Bauxite Residue (Red Mud). *Miner. Eng.* **2015**, *76*, 20–27. [CrossRef]
24. Bonomi, C.; Davris, P.; Balomenos, E.; Giannopoulou, I.; Panias, D. Ionometallurgical Leaching Process of Bauxite Residue: A Comparison between Hydrophilic and Hydrophobic Ionic Liquids. In Proceedings of the 35th International ICSOBA Conference, Hamburg, Germany, 2–5 October 2017; pp. 557–564.
25. Abbott, A.P.; Frisch, G.; Hartley, J.; Ryder, K.S. Processing of Metals and Metal Oxides Using Ionic Liquids. *Green Chem.* **2011**, *13*, 471. [CrossRef]
26. Vander Hoogerstraete, T.; Onghena, B.; Binnemans, K. Homogeneous Liquid–Liquid Extraction of Rare Earths with the Betaine—Betainium Bis(Trifluoromethylsulfonyl)Imide Ionic Liquid System. *Int. J. Mol. Sci.* **2013**, *14*, 21353–21377. [CrossRef] [PubMed]
27. Wellens, S.; Thijs, B.; Möller, C.; Binnemans, K. Separation of Cobalt and Nickel by Solvent Extraction with Two Mutually Immiscible Ionic Liquids. *Phys. Chem. Chem. Phys.* **2013**, *15*, 9663. [CrossRef] [PubMed]
28. Wasserscheid, P.; Keim, W. Ionic Liquids—New "Solutions" for Transition Metal Catalysis. *Angew. Chemie* **2000**, *39*, 3772–3789. [CrossRef]
29. Welton, T. Room-Temperature Ionic Liquids. Solvents for Synthesis and Catalysis. *Chem. Rev.* **1999**, *99*, 2071–2084. [CrossRef] [PubMed]
30. Bourbos, E.; Giannopoulou, I.; Karantonis, A.; Paspaliaris, I.; Panias, D. Electrodeposition of Rare Earth Metals from Ionic Liquids. In *Rare Earths Industry*; Elsevier: Amsterdam, The Netherlands, 2016; pp. 199–207.
31. Abbott, A.P.; McKenzie, K.J. Application of Ionic Liquids to the Electrodeposition of Metals. *Phys. Chem. Chem. Phys.* **2006**, *8*, 4265. [CrossRef] [PubMed]
32. Reddy, R.G. Emerging Technologies in Extraction and Processing of Metals. *Metall. Mater. Trans. B* **2003**, *34*, 137–152. [CrossRef]
33. Abbott, A.P.; Capper, G.; Davies, D.L.; Shikotra, P. Processing Metal Oxides Using Ionic Liquids. *Miner. Process. Extr. Metall.* **2006**, *115*, 15–18. [CrossRef]
34. Davris, P.; Balomenos, E.; Panias, D.; Paspaliaris, I. Selective Leaching of Rare Earth Elements from Bauxite Residue (Red Mud), Using a Functionalized Hydrophobic Ionic Liquid. *Hydrometallurgy* **2016**, *164*, 125–135. [CrossRef]
35. Binnemans, K.; Jones, P.T. Solvometallurgy: An Emerging Branch of Extractive Metallurgy. *J. Sustain. Metall.* **2017**, *3*, 570–600. [CrossRef]
36. Sajó, I.E. X-Ray Diffraction Quantitative Phase Analysis of Bayer Process Solids. In Proceedings of the 10th International Conference of ICSOBA, Bhubaneshwar, India, 23–30 November 2008; pp. 71–76.
37. Sajò, I.E. *XDB Powder Diffraction Phase Analytical System*, Version 3.107; Computer Software: Budapest, Hungary, 2005.
38. Vind, J.; Malfliet, A.; Bonomi, C.; Paiste, P.; Sajó, I.E.; Blanpain, B.; Tkaczyk, A.H.; Vassiliadou, V.; Panias, D. Modes of Occurrences of Scandium in Greek Bauxite and Bauxite Residue. *Miner. Eng.* **2018**, *123*, 35–48. [CrossRef]
39. Vind, J.; Malfliet, A.; Blanpain, B.; Tsakiridis, P.; Tkaczyk, A.; Vassiliadou, V.; Panias, D. Rare Earth Element Phases in Bauxite Residue. *Minerals* **2018**, *8*, 77. [CrossRef]